SUPPLEMENTAL MATERIAL

Table S1: Bioerosion Model Selection with all carbonate parameters: k is the number of parameters in the model, -log($\mathcal{L}$) is the negative log likelihood of the model, AIC_c is the Akaike Information Criterion corrected, ΔAIC_c is the difference from the lowest AIC_c value, R^2 is the proportion of total variance explained by the model, and Rank is the rank of the model with 1 representing the best fit. Each model is a linear regression of total bioerosion versus the means $(\overline{X})$ and variances $(Var(X))$ or covariance $(Cov(X))$ of each parameter. The Resource Availability Model includes DIN:DIP and chlorophyll *a* concentration and the Full Model includes means and variances or covariances for all listed environmental parameters. Environmental data are the residuals from a regression between each parameter versus log(depth) and distance from shore. Bioerosion rates were square-root transformed to meet model assumptions.The ranges for each environmental parameter are included in Silbiger et al. 2014.

	k	-log($\mathcal{L}$)	AICc	ΔAIC	R^2	Rank
pH	4.00	-13.24	-18.97	0.00	0.54	1
pCO_2	4.00	-12.02	-16.54	2.43	0.49	2
TA	4.00	-9.52	-11.55	7.43	0.34	3
DIC	4.00	-8.65	-9.79	9.18	0.28	4
Depth & Distance	4.00	-6.35	-5.19	13.78	0.09	5
Temperature	4.00	-6.11	-4.71	14.26	0.07	6
Resource Availability	6.00	7.44	-0.60	18.38	0.21	7
Full	18.00	-37.25	265.50	284.47	0.99	8

Detailed Methods:

Study site**:** Our study site is located in Kāne'ohe Bay, O'ahu on the windward (eastern) side of Moku o Lo'e (Coconut Island), adjacent to the Hawai'i Institute of Marine Biology; N21°25.975', W157°47.175'). This fringing reef is dominated by *Porites compressa* and *Montipora capitata*, with occasional colonies of *Pocillopora damicornis, Fungia scutaria,* and *Porites lobata*. Kāne'ohe Bay is a protected, semi-enclosed embayment; the residence time can be >1 month in the protected southern portion of Kāne'ohe Bay, where our study was located (Lowe et al., 2009a). Wave action is low (Smith et al., 1981; Lowe et al., 2009b,a), and currents are slow (5cm s^{-1} maximum) and tidally driven (mean and maximum tidal ranges are 0.7 and 1.1m, respectively) (Lowe et al., 2009b,a). Daily averages in pH, temperature, and O_2 in the Kāne'ohe Bay waters just offshore our site ranged from 7.83 - 8.03, 21.84-27.86 °C, and 5.82-7.81 mg L^{-1}, respectively, during our study period (Guadayol et al., 2014).

Environmental Parameters:

The discrete water samples were collected directly above each block within two days of spring tide at 08:00, 14:00, 20:00, and 02:00 on September 10-11, 2011, December 12-13, 2011, and April 4-5, 2012. All discrete water samples were collected on snorkel or SCUBA using 60 and 120ml plastic syringes. Syringes and storage vials were all pre-cleaned in a 10% HCl bath for 24 hours and rinsed three times with MilliQ water; during sample collection and processing syringes were rinsed three times with sample water. The environment was sampled more continuously for temperature and depth (sampling rate of ~ 0.1 min^{-1}) using one permanent and two mobile monitoring stations. Two mobile stations were deployed at a time, one on the reef flat and one on the reef slope, to get simultaneous measurements at two different blocks on the transect. Mobile stations (Sonde 600XLM, YSI Incorporated) were positioned 5 - 10cm above each block for a two-week period between May 2011 and March 2012. Blocks were sampled in random order, ensuring that the spatial gradient along the transect was not systematically confounded by temporal trends or seasonality (Guadayol et al., 2014). The permanent monitoring station (Sonde 6600-V2-4, YSI) was mounted to a pole a few meters away from the transect, downward facing at 1.7m depth over a 3m deep bottom, with sensors for temperature, depth, conductivity, pH, and O_2 to characterize the background water column conditions for the duration of the experiment. All multi-parametric probes were calibrated periodically using standard procedures and calibration solutions. The permanent station was recovered, cleaned, calibrated, and re-deployed 3 times during the study, and the mobile station probes were calibrated 7 times. Pre-calibration measurements of commercial standard solutions were conducted to detect sensor drift, although none was found for the period of study. Environmental data from the transect are reported in Silbiger et al. (2014)(Silbiger et al., 2014) and background water column data are reported in Guadayol et al. (2014) (Guadayol et al., 2014).

Nutrients and Chlorophyll: Water samples collected for nutrients were immediately filtered through combusted 25 mm diameter glass fiber filters (GF/F 0.2 µm) and transferred into 50 ml plastic centrifuge tubes. Nutrient samples were frozen and later analyzed for NO_3^-, NO_2^-, NH_4^+, and PO_4^{3-} on a Seal Analytical AA3 HR Nutrient Analyzer at the UH SOEST Laboratory for Analytical Chemistry. GF/F filters were folded in half, wrapped in aluminum foil, and frozen for chlorophyll a analysis using a Turner Designs 10AU Benchtop Fluorometer. The ratio of dissolved inorganic nitrogen to dissolved inorganic phosphate (DIN:DIP) was used as a proxy for resource quality available to filter feeders (Hauss et al., 2012), assuming that elemental composition of planktonic prey will be influenced by elemental composition of the water column, and was calculated from ([NO_3^-] + [NO_2^-] + [NH_4^+]):[PO_4^{3-}]) .

pH and TA: Mean and variance in pH at each block was calculated from water samples along the transect. Water samples for pH were immediately transferred into 25 ml borosilicate glass vials, brought to a constant temperature of 25°C in a water bath, and immediately analyzed using an m-cresol dye addition spectrophotometric technique and calibrated against a Tris buffer of known pH from the Dickson Laboratory at Scripps Institution of Oceanography. TA was fixed with 100 μL of $HgCl_2$ and analyzed using open cell potentiometric titrations on a Mettler T50 autotitrator and calibrated against a Certified Reference Material following Dickson et al. (2007) (Dickson et al., 2007) protocols. *In situ* pH and all other carbonate parameters were estimated using CO2SYS (van Heuven et al., 2011) with the following parameters: pH_t, TA, temperature, and salinity. The K1K2 dissociation constants were from Mehrbach (1973) (Mehrbach, 1973) (refit by Dickson and Millero (1987) (Dickson and Millero, 1987)) and HSO_4^- dissociation constants were taken from Uppstrom (1974) (Uppström, 1974) and Dickson (1990) (Dickson, 1990). Accuracy for TA and pH was better than 0.8% and 0.04%, respectively, and the precision was 3.55 µEq and 0.004 pH units.

Temperature: Temperature sensors (YSI 6560) were thermistors with manufacturer-reported accuracy of ±0.15°C and resolution of 0.01°C (YSI Incorporated 2011). Average differences in temperature along the transect were small and measured as a relative anomaly from the permanent station: $((\bar{x}_{mobile} - \bar{x}_{permanent})/\bar{x}_{permanent})$. To measure relative variability in temperature across the transect, we calculated the covariance in temperature between the mobile and permanent sensor arrays over a two-week period and compared this covariance across the transect.

Depth and Distance from Shore: Depth is the average depth measured at each block over the two week deployment of the mobile station. Distance from shore is the along-transect distance.

Turbulent Kinetic Energy Dissipation Rate (ϵ): Acoustic doppler velocimeters (Vectrino Field, Nortek A.S.) were deployed 5-10 cm above the blocks along with the multiparametric sondes measuring temperature and depth at 11 of the 21 stations. Unfortunately one of the velocimeters broke during deployment, and flow data could not be acquired for the rest of the stations and therefore was not included in the model selection. However, given the tight correlation between ϵ and distance from shore ($R^2 = 0.88$), distance from shore was used as a proxy for the hydrodynamic gradient.

Spikes were removed following a 3D phase-space thresholding technique Goring and Nikora (2002); Wahl

(2003) in the beam coordinates. Values with correlations <60 were also removed McLelland and Nicholas (2000). Gaps were linearly interpolated when shorter than 10 measurements. Empirical orthogonal functions (EOF) were used to align coordinates to streamwise/cross-stream axes for the entire sampling period

Turbulent kinetic energy dissipation rates (ϵ; m^2s^{-3}) for each segment were estimated from the spectra using the inertial subrange dissipation method Bluteau et al. (2011). Briefly, data was partitioned in 10 minutes intervals, the same sampling period as the multiparameter Sonde measuring temperature and depth. For each segment, data was further partitioned into 180 second segments of uninterrupted data, from which the fast Fourier transforms were obtained. A smoothed spectra was generated by averaging all the raw spectra. The inertial subrange was identified in the log transformed spectra as the segment that best fit a -5/3 model, with a minimum coefficient of determination (R^2) of 0.75, and encompassing at least one order of magnitude of frequencies. Fits were evaluated using F statistics and R^2. To account for the effect of advection by current and waves on the turbulent spectra, we used a generalized frozen turbulence model Lumley and Terray (1983). All calculations were done using MATLAB.

μCT:We used an eXplore CT120 μCT (GE Healthcare Xradia, Inc) at the Cornell University Imaging Multiscale CT Facility (Figure 2) to scan blocks before and after deployment (voltage = 100kV, current = 50mA). Angular projections were acquired in a full 360° rotation in 0.5° increments; two images at each angle were acquired and averaged creating a three-dimensional array of isotropic voxels at 50 μm^3 which was then averaged to 100 μm^3. Pre- and post-deployment scans were aligned, or registered, using an intensity-based image registration algorithm from the MATLAB ®Image Processing Toolbox. Mattes Mutual Information metric maximizes the number of corresponding pixels with similar intensity values (Mattes et al., 2001) which was used to describe the accuracy of the registration. We used the One Plus One Evolutionary Optimizer, an iterative algorithm that maximizes the best registration results by perturbing the parameters between iterations (Styner et al., 2000), as our optimization technique. A global threshold value was set at an intensity value of 200 to separate $CaCO_3$ from air and remove any effects of partial volume averaging at the coral block-air interface Silbiger et al. (2014). Intensity values are directly correlated with skeletal density at each pixel. The number of voxels exceeding this threshold was used in calculating secondary accretion and bioerosion. After the images were registered, both pre- and post-deployment scans were converted to binary, such that any positive intensity value (a pixel with $CaCO_3$) was assigned a one and all other values (air) were assigned a zero. The two images were then subtracted from one another giving a matrix of 1's, 0's, and -1's. I n the subtracted matrix, all pixels with a value of one represented areas of new $CaCO_3$ (accretion) and all values of negative one were areas where $CaCO_3$ was removed (bioerosion). A value of zero meant there was no change at that pixel between the before and after scans. Converting images to binary is the most conservative way to calculate secondary accretion and bioerosion; it does not account for any change in skeletal density, but rather an absolute loss of $CaCO_3$. Subtracting the two raw images, without converting to binary, would potentially over-estimate secondary accretion and bioerosion due to partial volume averaging of surrounding pixels or a change in skeletal density due to chemical dissolution. To calculate secondary accretion and bioerosion rates, all positive and negative values were summed in the subtracted matrix and multiplied by the voxel size (100 μm)^3 to give the total volume of $CaCO_3$ gained or lost, respectively. These values were then normalized to the surface area of the pre-deployment block and multiplied by the skeletal density and are expressed as kg $CaCO_3$ m^{-2} yr^{-1} for bioerosion and mm $CaCO_3$ yr^{-1} for secondary accretion. Bulk skeletal density of pre-deployment blocks was calculated using the buoyant weight technique. Surface area was calculated following methods by Legland et al. 2011Legland et al. (2011). Note that this volumetric analysis measures changes at the voxel scale of 100 μm^3, and, therefore, may underestimate bioerosion by microborers, which make erosion scars between 1 and 100 μm (Tribollet, 2008).

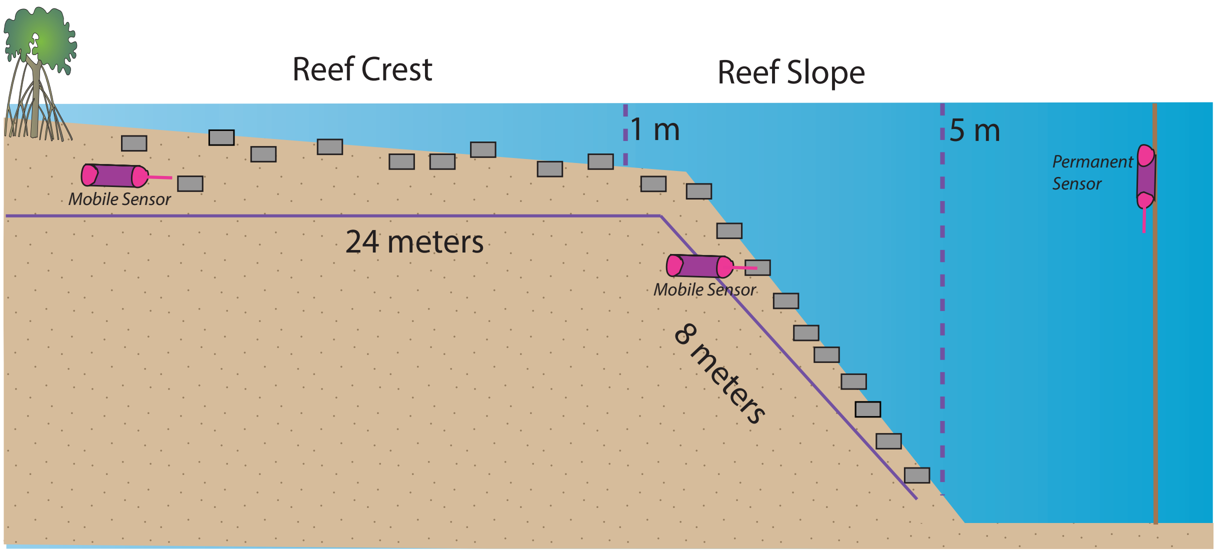

Figure S1: Schematic of reef transect. Experimental blocks (grey rectangles) were stratified between reef flat and reef slope along a 32 m transect and were deployed for one year. The depth ranged from 0.5 to 4.5 m. Discrete environmental samples were collected directly above each experimental block. Continuous sensors were stationed over each block for a minimum of two weeks (mobile sensors) and were normalized to a continuous time series from a permanent sensor station (Permanent sensors).

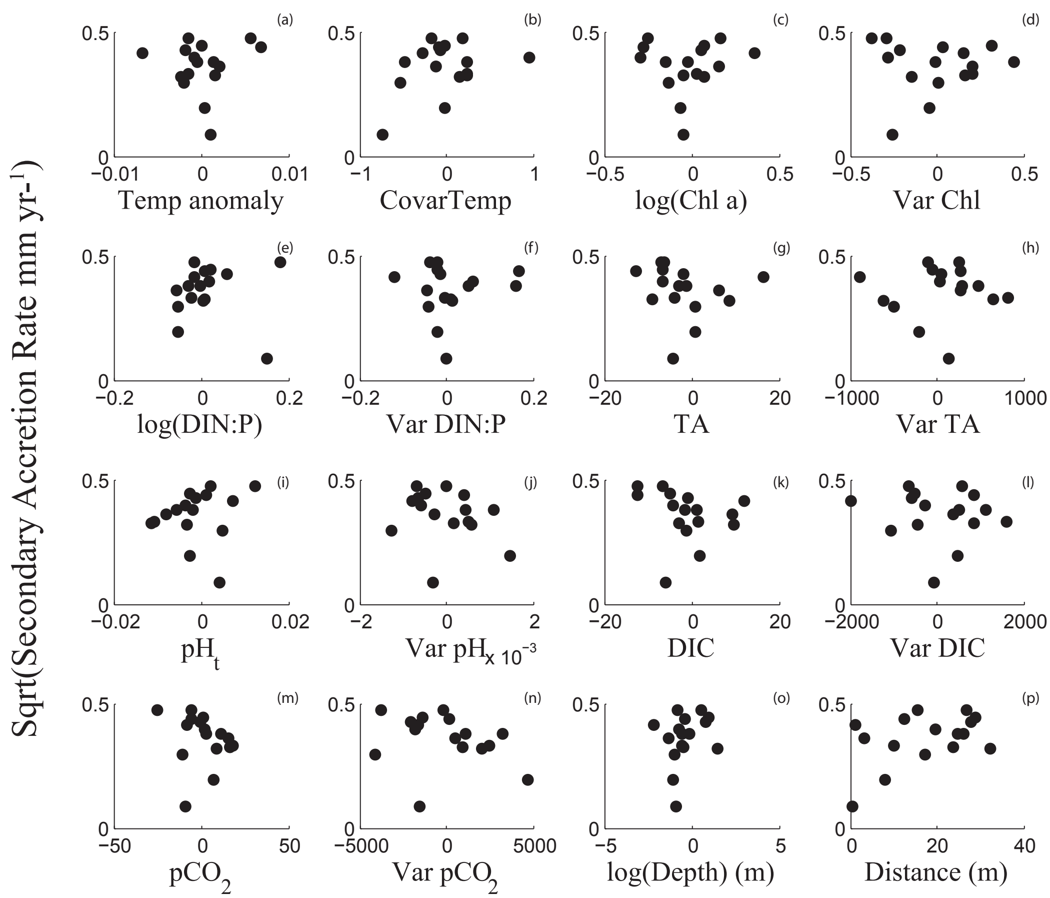

Figure S2: Secondary accretion versus the means and variances of all environmental parameters. Environmental parameters were regressed against log(depth) and distance from shore and the residuals from those regressions are used in this figure.

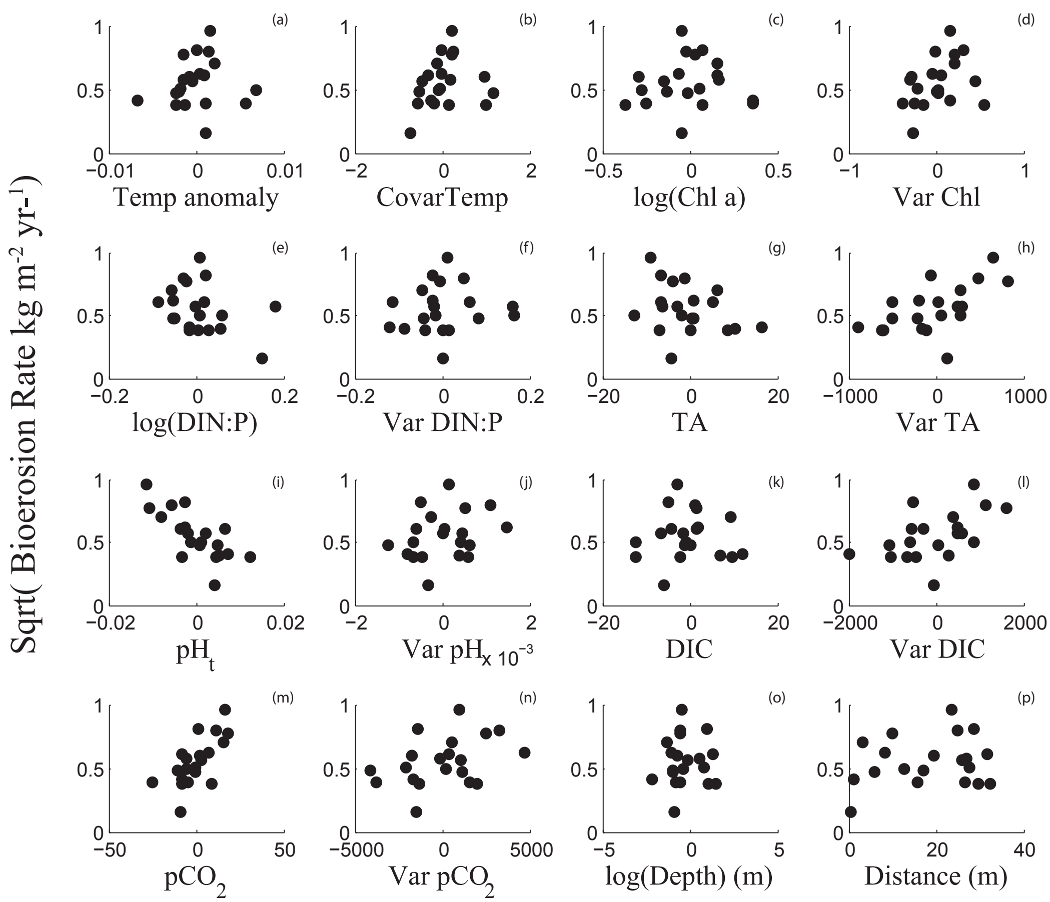

Figure S3: Bioerosion versus the means and variances of all environmental parameters. Environmental parameters were regressed against log(depth) and distance from shore and the residuals from those regressions are used in this figure.

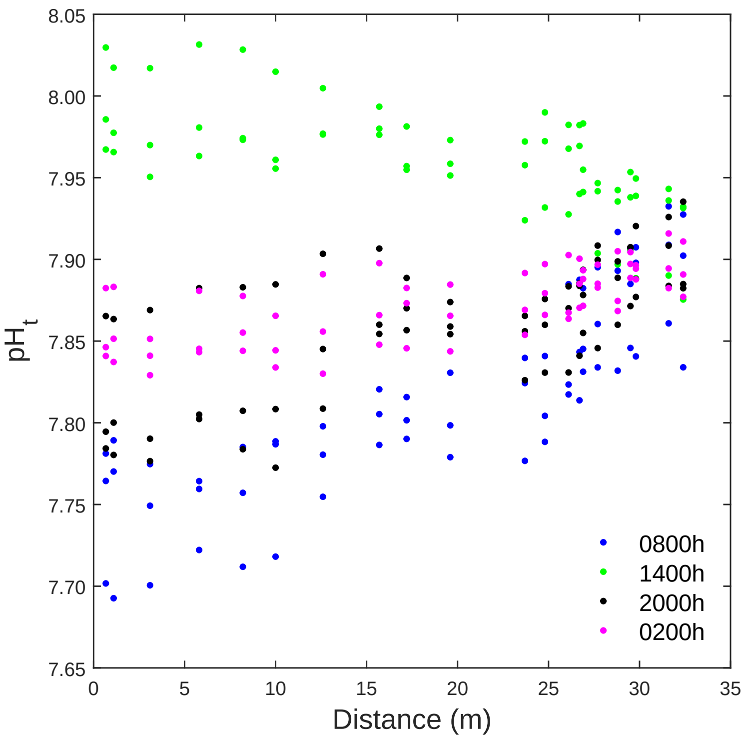

Figure S4: All discrete pH samples from September, December, and April sampling periods across the transect. In each sampling period, water samples were collected at 0800h (blue), 1400h (green), 2000h (black), and 0200h (magenta), resulting in 12 samples at each of the 21 blocks.

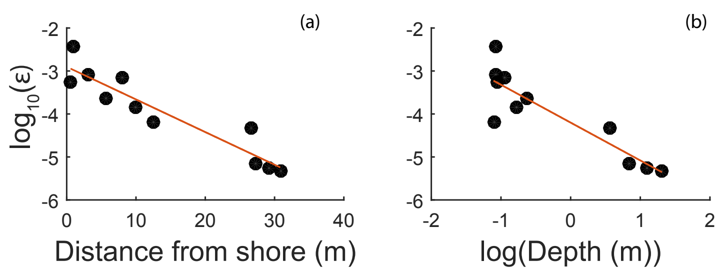

Figure S5: Turbulent kinetic energy dissipation rate (ϵ) (m^2s^{-3}) versus (a) distance from shore (b) and depth (n=11). Turbulence was measured at 11 of the 21 sites and there was a significant relationship between ϵ and distance from shore ($F_{11,9} = 63.1$, p<0.0001, R^2=0.88) and depth ($F_{11,9} = 35.0$, p=0.0002, R^2=0.80).

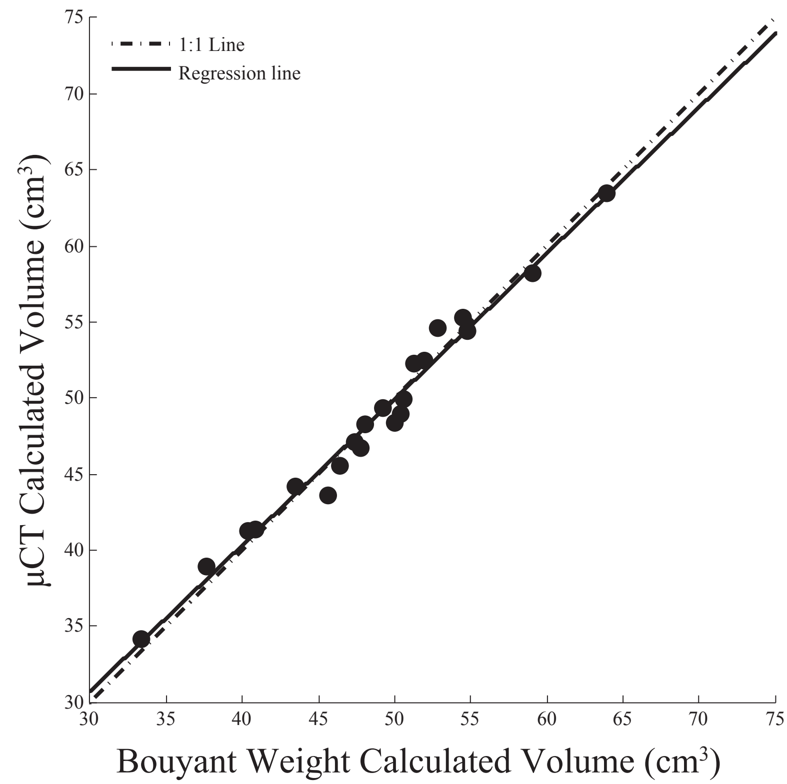

Figure S6: Comparison of calculated volumes (cm^3) using the buoyant weight and μCT methods described in this paper. Black circles are volumes calculated from the pre-deployment experimental blocks. We used a linear regression to test the relationship between the buoyant weight and μCT methods. The pre-deployment volumes calculated from each method are highly co-linear (F_{19} = 859, p<0.001, R = 0.98, $y = 0.96x + 1.9$)

Movie Legends

MovieS1: 3D visualization of μCT scan highlighting secondary accretion onto a block.

MovieS2: 3D visualization of μCT scan highlighting bioerosion from a block.

References

Bluteau, C. E., Jones, N. L., Ivey, G. N., 2011. Estimating turbulent kinetic energy dissipation using the inertial subrange method in environmental flows. Limnology and Oceanography: Methods 9 (7), 302–321.

Dickson, A., Millero, F., 1987. A comparison of the equilibrium constants for the dissociation of carbonic acid in seawater media. Deep Sea Research Part A. Oceanographic Research Papers 34 (10), 1733–1743.

Dickson, A., Sabine, C., Christian, J. R., 2007. Guide to Best Practices for Ocean CO_2 Measurements. PICES Special Publication 3.

Dickson, A. G., 1990. Standard potential of the reaction:$AgCl(s) + 12H2(g) = Ag(s) + HCl(aq)$, and and the standard acidity constant of the ion HSO_4^- in synthetic sea water from 273.15 to 318.15 k. The Journal of Chemical Thermodynamics 22 (2), 113–127.

Goring, D. G., Nikora, V. I., 2002. Despiking acoustic doppler velocimeter data. Journal of Hydraulic Engineering 128 (1), 117–126.

Guadayol, Ò., Silbiger, N. J., Donahue, M. J., Thomas, F. I., 2014. Patterns in temporal variability of temperature, oxygen and pH along an environmental gradient in a coral reef. Plos One 9 (1), e85213.

Hauss, H., Franz, J., Sommer, U., 2012. Changes in N: P stoichiometry influence taxonomic composition and nutritional quality of phytoplankton in the Peruvian upwelling. J Sea Res 73, 74–85.

Legland, D., Kiêu, K., Devaux, M.-F., 2011. Computation of minkowski measures on 2d and 3d binary images. Image Analysis & Stereology 26 (2), 83–92.

Lowe, R. J., Falter, J. L., Monismith, S. G., Atkinson, M. J., 2009a. A numerical study of circulation in a coastal reef-lagoon system. J. Geophys. Res. 114 (C6), C06022.

Lowe, R. J., Falter, J. L., Monismith, S. G., Atkinson, M. J., 2009b. Wave-driven circulation of a coastal reef-lagoon system. J. Phys. Oceanogr. 39 (4), 873–893.

Lumley, J., Terray, E., 1983. Kinematics of turbulence convected by a random wave field. Journal of Physical Oceanography 13 (11), 2000–2007.

Mattes, D., Haynor, D., Vesselle, H., Lewellen, T. K., W, E., 2001. Non-rigid multimodality image registration. Medical Imaging 2001: Image Processing, 1609–1620.

McLelland, S. J., Nicholas, A. P., 2000. A new method for evaluating errors in high-frequency ADV measurements. Hydrological Processes 14 (2), 351–366.

Mehrbach, C., 1973. Measurement of the apparent dissociation constants of carbonic acid in seawater at atmospheric pressure. Limnol. Oceanogr. 18, 897–907.

Silbiger, N. J., Guadayol, Ò., Thomas, F. I., Donahue, M. J., 2014. Reefs shift from net accretion to net erosion along a natural environmental gradient. Marine Ecology Progress Series 515, 33–44.

Smith, S. V., Kimmerer, W. J., Laws, E. A., Brock, R. E., Walsh, T. W., 1981. Kaneohe Bay sewage diversion experiment- perspectives on ecosystem responses to nutritional perturbation. Pac. Sci. 35 (4), 279–402.

Styner, M., Brechbuhler, C., Szckely, G., Gerig, G., 2000. Parametric estimate of intensity inhomogeneities applied to mri. Medical Imaging, IEEE Transactions on 19 (3), 153–165.

Tribollet, A., 2008. Current Developments in Bioerosion. Springer-Verlag Berlin Heudelberg, Ch. The boring microflora in modern coral reef ecosystems: a review of its roles, pp. 67–94.

Uppström, L. R., 1974. The boron/chlorinity ratio of deep-sea water from the pacific ocean. In: Deep Sea Research and Oceanographic Abstracts. Vol. 21. pp. 161–162.

van Heuven, S., Pierrot, D., Rae, J., Lewis, E., Wallace, D., 2011. MATLAB Program Developed for CO2 System Calculations. ORNL/CDIAC-105b. Carbon Dioxide Information Analysis Center, Oak Ridge National Laboratory, U.S. Department of Energy, Oak Ridge, Tennessee.

Wahl, T. L., 2003. Discussion of "Despiking acoustic doppler velocimeter data" by Derek G. Goring and Vladimir I. Nikora. Journal of Hydraulic Engineering 129 (6), 484–487.